

## EFFECT OF STRAIN RATE ON DUCTILE FRACTURE. A NEW METHODOLOGY<sup>1</sup>

WOJCIECH K. NOWACKI, ZDZISŁAW NOWAK  
PIOTR PERZYNA, RYSZARD B. PEŁCHERSKI

*Institute of Fundamental Technological Research, Polish Academy of Sciences, Warsaw, Poland*  
*e-mail: znowak@ippt.gov.pl; pperzyna@ippt.gov.pl; rpecher@ippt.gov.pl*

The aim of our study is to discuss a new methodology to account for the effect of strain rate on ductile fracture phenomena. Theory of inelastic materials accounting for the effects of microshear bands and microdamage is presented. The influence of microshear bands is explained by means of a function describing the instantaneous contribution of shear banding in the total rate of plastic deformation. The experimental investigations of the effect of strain rate on ductile fracture with use of the results of a dynamic double shear test of DH-36 steel with thermographic observations are reported. The registration of temperature evolution during the deformation process can provide additional data for the identification of the shear banding contribution function and the onset of ductile fracture.

*Key words:* effect of strain rate, ductile fracture, dynamic double shear test, DH-36 steel, thermographic observation

### 1. Introduction

The effect of impact loading and strain rate on failure, in particular on ductile fracture of metals, is one of less understood phenomena in thermo-mechanics of solids. Phenomenological failure criteria are often considered, in which the critical failure strain depends on an accumulated equivalent strain and strain rate, which is usually averaged over a certain gage volume. Sometimes, a

---

<sup>1</sup>This is an extended version of the joint contribution with Wojciech K. Nowacki published in the *Proceedings of the Workshop in Memory of Prof. J.R. Klepaczko*, May 13-15, 2009, Metz, ed. by A. Rusinek and P. Chevrier, LaBPS ENIM and LPMM University of Metz

stress triaxiality parameter and an internal variable representing microdamage are included, c.f. e.g. Arias *et al.* (2008), Perzyna (2005). The analysis of the results of recent studies show that an adequate prediction of dynamic fracture processes should account for physical mechanisms activated on different levels of observation. In particular, the multiscale mechanism of shear banding plays pivotal role in evolution of ductile fracture. Although the effects of shear banding were implemented in the phenomenological models of plasticity and viscoplasticity (Pęcherski, 1998; Nowak *et al.*, 2007), however these phenomena were not accounted for the modelling of ductile fracture processes. Furthermore, in numerical simulations of inelastic deformations in solids subjected to dynamic loading conditions, a very fine finite element mesh is necessary to account for the effects of adiabatic microshear banding, what increases remarkably costs of computations, cf. Klepaczko *et al.* (2009).

The aim of our paper is to formulate theoretical foundations and to propose an outline of a new methodology to account for the effect of strain rate on ductile fracture phenomena. The influence of the multi-scale hierarchy of shear bands which develop during advanced plastic strains is described by means of a scalar function describing locally the instantaneous contribution of shear banding in the total rate of plastic deformation, cf. Pęcherski (1998), Nowak *et al.* (2007), Kowalczyk-Gajewska and Pęcherski (2009). In Nowacki *et al.* (2007), experimental investigations of the effect of strain rate on ductile fracture with use of the results of a dynamic double shear test of DH-36 steel associated with thermographic observations were reported. The registration of temperature evolution during the process provides additional data, which can be used for the identification of the shear banding contribution function by the solution of a certain inverse problem, in which the numerical simulation of thermo-mechanical process simulating the performed test is implemented, cf. Fraś *et al.* (2010). Also the general scheme of determination of the fracture model to the investigated experimentally material (DH-36 steel) was presented.

## 2. Experimental foundations

### 2.1. Double shear tests

Let us consider the double shear test of the DH-36 steel sheet in quasi-static as well as in dynamic loading conditions. This kind of test, proposed in Gary and Nowacki (1994) as an elaboration of Yoshida and Myauchi (1978) idea of

"double shear" specimen, was chosen to illustrate the proposed methodology of analysing the strain rate effect on ductile fracture. A simple shear test is particularly attractive, since the application of this type of loading path can result in large strains without the occurrence of plastic instability. The mechanical characteristics and the temperature distributions of the sample surface obtained by a thermovision camera during the deformation processes were recorded, processed and stored in the computerized registration system. Investigations of the initiation and further development of fracture locus at various strain rates using the infrared technique were performed. In the case of dynamic loading, the Split Hopkinson Pressure Bar (SHPB) was used. The scheme of the applied shear device is shown in Fig. 1a. A new shear device was used by Gary and Nowacki (1994) to perform tests under high strain rates on specimens having the form of metal sheets. The loading and the displacements of this device are controlled by the SHPB acting in compression. The role of the special device is to transform the compression into a plane shear.

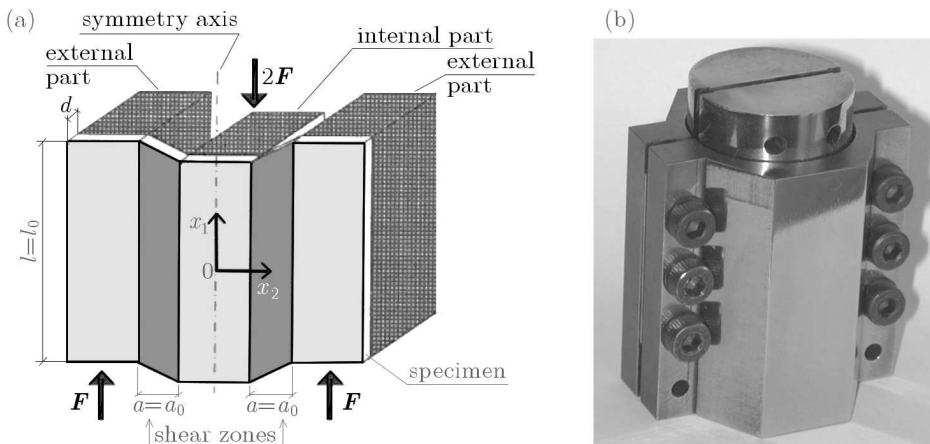


Fig. 1. (a) Scheme of shear testing – two shear zones, (b) shear device

The shear device for investigations at high strain rates as well as in quasi-static conditions consists of two coaxial cylindrical parts: the external tubular part and the internal massive part (see Fig. 1b). Both cylinders are divided into two symmetrical parts, and between them the sheet to be tested is fixed.

Two boundaries of the specimen between the internal and external parts of the device are in plane shear when these cylinders move axially one toward the other, Fig. 2.

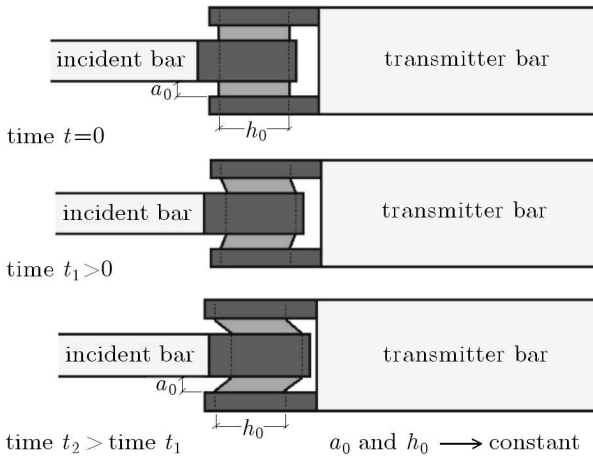


Fig. 2. Scheme of simple shear. Loading and displacement are controlled by SHPB acting in compression

The highest strain rate in the specimen was obtained with application of one bar of the SHPB system. In this experimental technique, the flat projectile strikes directly the double shear specimen placed in the device in front of the transmitting bar. The details of proper dimensioning of the specimen are given in Nowacki *et al.* (2007). In our case, the material sheet has a nominal thickness of 0.64 mm. In the case of dynamic test at high strain rates, the specimens of the strain gauge length 20 mm were used (cf. Rusinek *et al.*, 2002). Design of the specimen for dynamic testing in simple shear is presented in Fig. 3.

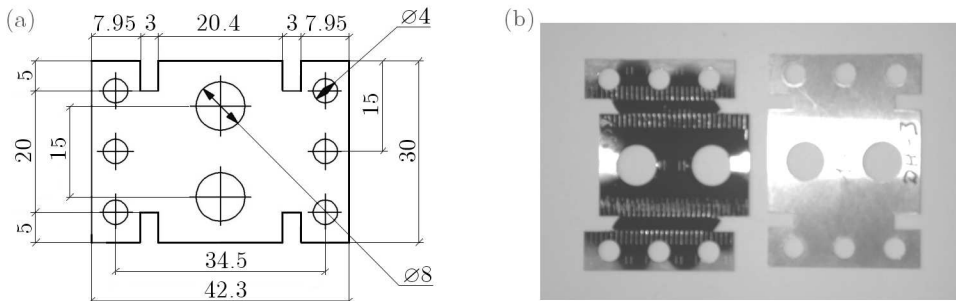


Fig. 3. (a) Scheme of the specimen used in double shear tests, (b) specimen after and before simple shear deformation

### 2.2. Quasi-static tests in simple shear

Deformation processes always modify temperature fields in materials while temperature variations influence the stress-strain characteristic. Strong effects

of the thermo-mechanical coupling are observed during the process of the simple shear test. During this test, the first invariant of stress tensor  $\Delta\sigma_{ii} = 0$ , thus, in elastic range of deformation temperature does not change, Kelvin (1853). The following plastic deformation is accompanied by an increase in temperature. It is caused by transformation of a significant part of the plastic energy into heat, Rusinek *et al.* (2002). The goal of our investigation was obtaining the mechanical characteristics of the material as well as the temperature distributions in the shear areas. The samples were placed in a specially designed grip for quasi-static tests, transforming the compression into a simple shear process (Fig. 4a). The grip was fitted in the testing machine, working in the compression mode. A change of temperature of the surface of two shear paths has been observed in situ during the test.

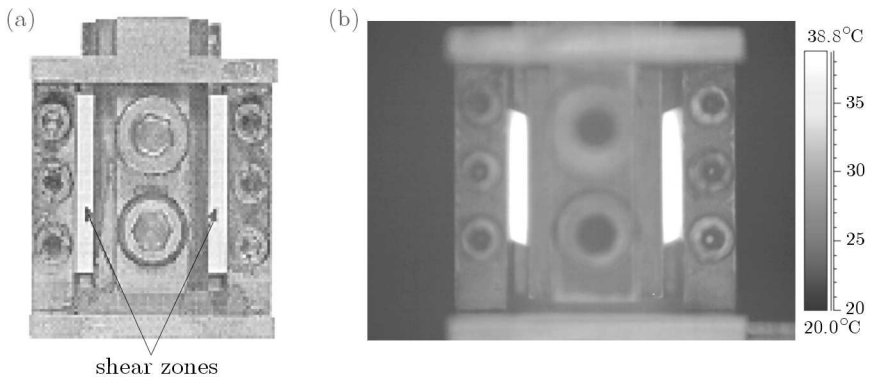


Fig. 4. (a) Photograph of the shear test device, (b) example of thermogram obtained during the simple shear test of DH-36 steel

The tests were performed at room temperature (295 K), with the shear strain rates equal to  $10^{-3} \text{ s}^{-1}$ ,  $10^{-1} \text{ s}^{-1}$  and  $10^0 \text{ s}^{-1}$ . During deformation, the load vs. crosshead displacement and the distribution of infrared radiation, emitted by the specimen, were continuously registered. The distribution was measured using the thermovision camera coupled with a computer system of data acquisition and conversion. The mechanical characteristics made it possible to derive the stress-strain relations. The distribution of intensity of the infrared radiation registered in the same time allowed us to reconstruct thermal pictures (Fig. 4b) of the samples and, in this way, to find the temperature changes of the sample subjected to shear test. The mean-square error of temperature evaluation was about 0.2-0.5 K. In order to ensure higher and more homogeneous emissivity, the surfaces of the shear zones of the steel sheet specimens were blackened with a carbon powder. As a result of the study,

we have obtained stress-strain and temperature-strain characteristics. See, for example, Fig. 5a and Fig. 5b at shear strain rates  $10^{-1} \text{ s}^{-1}$  and  $1 \text{ s}^{-1}$ .

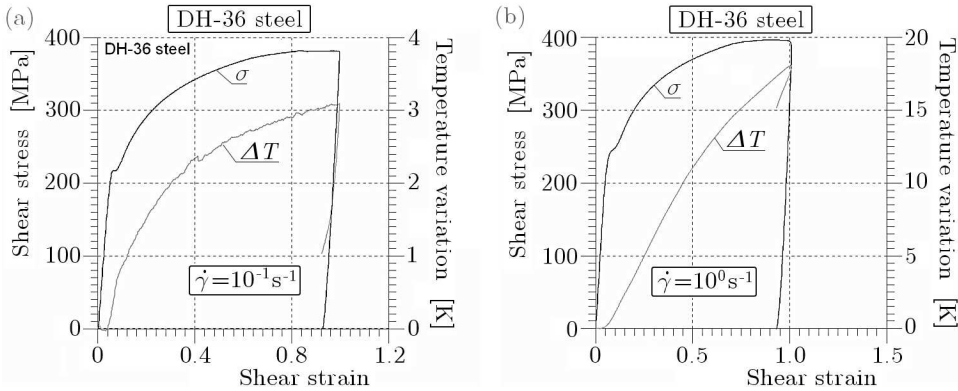


Fig. 5. (a) Stress-strain and mean temperature changes curves of DH-36 steel at the rate of deformation equal  $10^{-1} \text{ s}^{-1}$ ; (b) stress-strain and mean temperature changes curves of DH-36 steel at the rate of deformation equal  $1 \text{ s}^{-1}$

For the DH-36 steel, temperature does not change in the elastic range of shear. The rapid increments of temperature are observed in the region of plastic deformation. The temperature increases with an increase of the rate of deformation. During unloading, the temperature smoothly decreases due to the heat transmission to the grips and surroundings.

### 2.3. Dynamic tests in simple shear at high strain rates

The device with the double-shear specimen is placed between two bars of the SHPB (Fig. 6). The mechanical impedance of the shear device and the SHPB must be the same to avoid the noise in the interface signal (cf. Nowacki, 2001). The impulse is created by the third projectile bar. The impact velocity is measured by the set-up consisting of three sources of light and three independent photodiodes. The time interval during crossing of a projectile by two rays of light is recorded by the time counter. The impulses are registered at the strain resistance gauges.

The comparison of the shear stress-shear strain curves in the case of dynamic loading (direct impact test) at the shear strain rate  $6.3 \cdot 10^3 \text{ s}^{-1}$  with quasi-static curves is shown in Fig. 7.

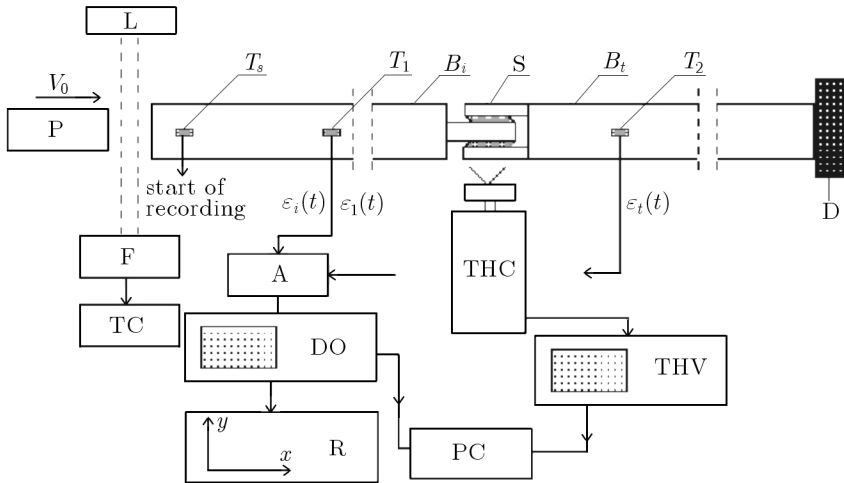


Fig. 6. Standard SHPB apparatus; P – projectile,  $B_i$  – incident bar,  $B_t$  – transmitting bar, S – shear device with double shear specimen, D – damper, L – source of light, F – photodiodes, TC – time counter,  $T_1$ ,  $T_2$  and  $T_s$  – strain gauges, A – amplifier, DO – digital oscilloscope, PC – microcomputer, R –  $xy$  recorder or graphic printer, THC – thermo-vision camera, THV – oscilloscope of thermo-vision set

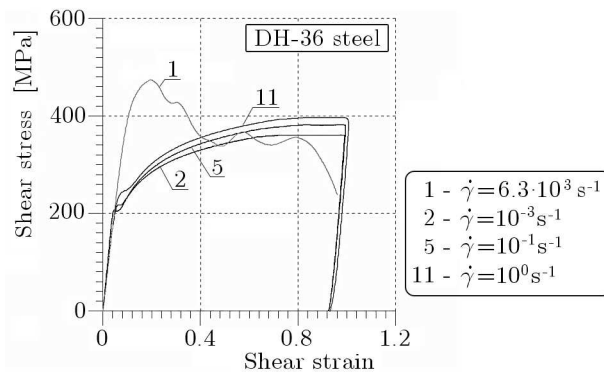


Fig. 7. Comparison of stress-strain curves obtained in quasi-static and dynamic shear tests

### 3. Thermo-elasto-viscoplastic model of a material

#### 3.1. Basic assumptions and definitions

Let us assume that a continuum body is an open bounded set  $\mathcal{B} \subset \mathbb{R}^3$ , and let  $\phi : \mathcal{B} \rightarrow \mathcal{S}$  be a  $C^1$  configuration of  $\mathcal{B}$  in  $\mathcal{S}$ . The tangent of  $\phi$  is denoted  $\mathbf{F} = T\phi$  and is called the deformation gradient of  $\phi$ .

Let  $\{X^A\}$  and  $\{x^a\}$  denote coordinate systems on  $\mathcal{B}$  and  $\mathcal{S}$ , respectively. Then we refer to  $\mathcal{B} \subset \mathbb{R}^3$  as the reference configuration of a continuum body with particles  $\mathbf{X} \in \mathcal{B}$  and to  $\mathcal{S} = \phi(\mathcal{B})$  as the current configuration with points  $\mathbf{x} \in \mathcal{S}$ . The matrix  $\mathbf{F}(\mathbf{X}, t) = \partial\phi(\mathbf{X}, t)/\partial\mathbf{X}$  with respect to the coordinate bases  $\mathbf{E}_A(\mathbf{X})$  and  $\mathbf{e}_a(\mathbf{x})$  is given by

$$F_A^a(\mathbf{X}, t) = \frac{\partial\phi^a}{\partial X^A}(\mathbf{X}, t) \tag{3.1}$$

where the mapping  $\mathbf{x} = \phi(\mathbf{X}, t)$  represents motion of the body  $\mathcal{B}$ .

We consider the local multiplicative decomposition

$$\mathbf{F} = \mathbf{F}^e \mathbf{F}^p \tag{3.2}$$

where  $(\mathbf{F}^e)^{-1}$  is the deformation gradient that releases elastically the stress on the neighbourhood  $\phi(\mathcal{N}(\mathbf{X}))$  in the current configuration.

Let us define the total and elastic Finger deformation tensors

$$\mathbf{b} = \mathbf{F}\mathbf{F}^\top \qquad \mathbf{b}^e = \mathbf{F}^e \mathbf{F}^{e\top} \tag{3.3}$$

respectively, and the Eulerian strain tensors as follows

$$\mathbf{e} = \frac{1}{2}(\mathbf{g} - \mathbf{b}^{-1}) \qquad \mathbf{e}^e = \frac{1}{2}(\mathbf{g} - \mathbf{b}^{e-1}) \tag{3.4}$$

where  $\mathbf{g}$  denotes the metric tensor in the current configuration.

By definition (cf. Perzyna, 1995)

$$\mathbf{e}^p = \mathbf{e} - \mathbf{e}^e = \frac{1}{2}(\mathbf{b}^{e-1} - \mathbf{b}^{-1}) \tag{3.5}$$

we introduce the plastic Eulerian strain tensor.

To define objective rates for vectors and tensors, we use the Lie derivative (cf. Marsden and Hughes, 1983). Let us define the Lie derivative of a spatial tensor field  $\mathbf{t}$  with respect to the velocity field  $\mathbf{v}$  as

$$L_{\mathbf{v}}\mathbf{t} = \phi_* \frac{\partial}{\partial t}(\phi^*\mathbf{t}) \tag{3.6}$$

where  $\phi^*$  and  $\phi_*$  denote the pull-back and push-forward operations, respectively.

The rate of deformation tensor is defined as follows

$$\mathbf{d}^p = L_{\mathbf{v}}\mathbf{e}^p = \frac{1}{2}L_{\mathbf{v}}\mathbf{g} = \frac{1}{2}(g_{ac}v^c|_b + g_{cb}v^c|_a)\mathbf{e}^a \otimes \mathbf{e}^b \tag{3.7}$$

where the symbol  $\flat$  denotes the index lowering operator and  $\otimes$  the tensor product

$$v^a|_b = \frac{\partial v^a}{\partial x^b} + \gamma_{bc}^a v^c \quad (3.8)$$

and  $\gamma_{bc}^a$  denotes the Christoffel symbol for the general coordinate systems  $\{x^a\}$ . The components of the spin  $\omega$  are given by

$$\omega_{ab} = \frac{1}{2}(g_{ac}v^c|_b - g_{cb}v^c|_a) = \frac{1}{2}\left(\frac{\partial v_a}{\partial x^b} - \frac{\partial v_b}{\partial x^a}\right) \quad (3.9)$$

Similarly

$$\mathbf{d}^{e^b} = L_{\mathbf{v}}\mathbf{e}^{e^b} \quad \mathbf{d}^{p^b} = L_{\mathbf{v}}\mathbf{e}^{p^b} \quad (3.10)$$

and

$$\mathbf{d} = \mathbf{d}^e + \mathbf{d}^p \quad (3.11)$$

Let  $\boldsymbol{\tau}$  denote the Kirchhoff stress tensor related to the Cauchy stress tensor  $\boldsymbol{\sigma}$  by

$$\boldsymbol{\tau} = J\boldsymbol{\sigma} = \frac{\rho_{Ref}}{\rho}\boldsymbol{\sigma} \quad (3.12)$$

where the Jacobian  $J$  is the determinant of the linear transformation  $\mathbf{F}(\mathbf{X}, t) = (\partial/\partial\mathbf{X})\phi(\mathbf{X}, t)$ ,  $\rho_{Ref}(\mathbf{X})$  and  $\rho(\mathbf{x}, t)$  denote the mass density in the reference and current configuration, respectively.

### 3.2. Constitutive postulates

Let us assume that: (i) conservation of mass, (ii) balance of momentum, (iii) balance of moment of momentum, (iv) balance of energy, (v) entropy production inequality hold.

We base on the fundamental postulates already presented in the paper of Perzyna (2005) (see details) and we assume that the evolution equation for the internal state variable vector  $\boldsymbol{\mu}$  is assumed in the form as follows

$$L_{\mathbf{v}}\boldsymbol{\mu} = \widehat{\mathbf{m}}(\mathbf{e}, \mathbf{F}, \vartheta, \boldsymbol{\mu}) \quad (3.13)$$

where the evolution tensor function  $\widehat{\mathbf{m}}$  has to be determined based on careful physical interpretation of a set of the internal state variables and analysis of available experimental observations.

For our practical purposes, it is sufficient to assume that the internal state vector  $\boldsymbol{\mu}$  has the form

$$\boldsymbol{\mu} = (\epsilon^p, \xi) \quad (3.14)$$

where  $\epsilon^P$  is the equivalent viscoplastic deformation, i.e.

$$\epsilon^P = \int_0^t \sqrt{\frac{2}{3} \mathbf{d}^P : \mathbf{d}^P} dt \tag{3.15}$$

and  $\xi$  is volume fraction porosity and takes into account micro-damaged effects.

Let us introduce the plastic potential function  $f = f(J_1, J_2, \vartheta, \boldsymbol{\mu})$ , where  $J_1, J_2$  denote the first two invariants of the Kirchhoff stress tensor  $\boldsymbol{\tau}$ .

Let us postulate the evolution equations as follows

$$\mathbf{d}^P = \Lambda \mathbf{P} \qquad \dot{\xi} = \Xi \tag{3.16}$$

where for the elasto-viscoplastic model of a material we assume (cf. Perzyna, 1963, 1966)

$$\Lambda = \frac{1}{T_m} \left\langle \Phi \left( \frac{f}{\kappa} - 1 \right) \right\rangle \tag{3.17}$$

$T_m$  denotes the relaxation time for mechanical disturbances, the isotropic work-hardening-softening function  $\kappa$  is

$$\kappa = \widehat{\kappa}(\epsilon^P, \vartheta, \xi) \tag{3.18}$$

$\Phi$  is the empirical overstress function, the bracket  $\langle \cdot \rangle$  defines the ramp function

$$\mathbf{P} = \frac{\partial f}{\partial \boldsymbol{\tau}} \Big|_{\xi = \text{const}} \left( \left\| \frac{\partial f}{\partial \boldsymbol{\tau}} \right\| \right)^{-1} \tag{3.19}$$

$\Xi$  denotes the evolution function which has to be determined.

### 3.3. Intrinsic micro-damage mechanisms

To take into consideration experimentally observed time dependent effects it is advantageous to use the proposition of the description of the intrinsic micro-damage process presented by Perzyna (1986) and Duszek-Perzyna and Perzyna (1994).

Let us assume that the intrinsic micro-damage process consists of the nucleation and growth mechanisms.

Physical considerations (cf. Curran *et al.*, 1987; Perzyna, 1986) have shown that the nucleation of microvoids in dynamic loading processes, which are characterised by very short time duration, is governed by the thermally-activated mechanism. Based on this heuristic suggestion and taking into account the

influence of the stress triaxiality on the nucleation mechanism, we postulate for the rate dependent plastic flow

$$(\dot{\xi})_{nucl} = \frac{1}{T_m} h^*(\xi, \vartheta) \left[ \exp \frac{m^*(\vartheta) |I_n - \tau_n(\xi, \vartheta, \epsilon^p)|}{k\vartheta} - 1 \right] \quad (3.20)$$

where  $k$  denotes the Boltzmann constant,  $h^*(\xi, \vartheta)$  represents the void nucleation material function which is introduced to take account of the effect of microvoid interaction,  $m^*(\vartheta)$  is a temperature dependent coefficient,  $\tau_n(\xi, \vartheta, \epsilon^p)$  is the porosity, temperature and equivalent plastic strain dependent threshold stress for microvoid nucleation

$$I_n = a_1 J_1 + a_2 \sqrt{J'_2} + a_3 \sqrt[3]{J'_3} \quad (3.21)$$

defines the stress intensity invariant for nucleation,  $a_i$  ( $i = 1, 2, 3$ ) are material constants,  $J_1$  denotes the first invariant of the Kirchhoff stress tensor  $\boldsymbol{\tau}$ ,  $J'_2$  and  $J'_3$  are the second and third invariants of the stress deviator  $\boldsymbol{\tau}'$ .

For the growth mechanism, we postulate (cf. Johnson, 1981; Perzyna, 1986; Dornowski and Perzyna, 2000)

$$(\dot{\xi})_{grow} = \frac{1}{T_m} \frac{g^*(\xi, \vartheta)}{\kappa_0} [I_g - \tau_{eq}(\xi, \vartheta, \epsilon^p)] \quad (3.22)$$

where  $T_m \kappa_0$  denotes the dynamic viscosity of a material,  $g^*(\xi, \vartheta)$  represents the void growth material function and takes account for void interaction,  $\tau_{eq}(\xi, \vartheta, \epsilon^p)$  is the porosity, temperature and equivalent plastic strain dependent void growth threshold stress

$$I_g = b_1 J_1 + b_2 \sqrt{J'_2} + b_3 \sqrt[3]{J'_3} \quad (3.23)$$

defines the stress intensity invariant for growth and  $b_i$  ( $i = 1, 2, 3$ ) are material constants.

Finally, the evolution equation for the porosity  $\xi$  has the form

$$\begin{aligned} \dot{\xi} = & \frac{h^*(\xi, \vartheta)}{T_m} \left[ \exp \frac{m^*(\vartheta) |I_n - \tau_n(\xi, \vartheta, \epsilon^p)|}{k\vartheta} - 1 \right] + \\ & + \frac{g^*(\xi, \vartheta)}{T_m \kappa_0} [I_g - \tau_{eq}(\xi, \vartheta, \epsilon^p)] \end{aligned} \quad (3.24)$$

To have consistent theory of elasto-viscoplasticity, we can replace the exponential function in the nucleation term and the linear function in the growth

term by the empirical overstress  $\bar{\Phi}$ , then the evolution equation for the porosity  $\xi$  takes the form as follows (cf. Perzyna, 2005)

$$\begin{aligned} \dot{\xi} = & \frac{1}{T_m} h^*(\xi, \vartheta) \left\langle \bar{\Phi} \left[ \frac{I_n}{\tau_n(\xi, \vartheta, \epsilon^p)} - 1 \right] \right\rangle + \\ & + \frac{1}{T_m} g^*(\xi, \vartheta) \left\langle \bar{\Phi} \left[ \frac{I_g}{\tau_n(\xi, \vartheta, \epsilon^p)} - 1 \right] \right\rangle \end{aligned} \tag{3.25}$$

This determines the evolution function  $\Xi$ .

### 3.4. Thermodynamic restrictions and rate type constitutive equations

Suppose the axiom of the entropy production holds. Then the constitutive assumption on the existence of the free energy function and evolution equations (3.16) lead to the results as follows

$$\begin{aligned} \boldsymbol{\tau} = \rho_{Ref} \frac{\partial \hat{\psi}}{\partial \mathbf{e}} \quad \eta = - \frac{\partial \hat{\psi}}{\partial \vartheta} \\ - \frac{\partial \hat{\psi}}{\partial \boldsymbol{\mu}} L_v \boldsymbol{\mu} - \frac{1}{\rho \vartheta} \mathbf{q} \text{grad } \vartheta \geq 0 \end{aligned} \tag{3.26}$$

where  $\mathbf{q}$  is the heat flux vector.

The rate of internal dissipation is determined by

$$\vartheta \dot{i} = - \frac{\partial \hat{\psi}}{\partial \boldsymbol{\mu}} L_v \boldsymbol{\mu} = - \left( \frac{\partial \hat{\psi}}{\partial \epsilon^p} \sqrt{\frac{2}{3}} \right) \Lambda - \frac{\partial \hat{\psi}}{\partial \xi} \Xi \tag{3.27}$$

Operating on the stress relation Eq. (3.26)<sub>1</sub> with the Lie derivative and keeping the internal state vector constant, we obtain (cf. Duszek-Perzyna and Perzyna, 1994)

$$L_v \boldsymbol{\tau} = \mathcal{L}^e : \mathbf{d} - \mathcal{L}^{th} \dot{\vartheta} - [(\mathcal{L}^e + \mathbf{g}\boldsymbol{\tau} + \boldsymbol{\tau}\mathbf{g}) : \mathbf{P}] \frac{1}{T_m} \left\langle \bar{\Phi} \left( \frac{f}{\kappa} - 1 \right) \right\rangle \tag{3.28}$$

where

$$\mathcal{L}^e = \rho_{Ref} \frac{\partial^2 \hat{\psi}}{\partial \mathbf{e}^2} \quad \mathcal{L}^{th} = - \rho_{Ref} \frac{\partial^2 \hat{\psi}}{\partial \mathbf{e} \partial \vartheta} \tag{3.29}$$

Substituting  $\dot{\psi}$  into the energy balance equation and taking into account the results from Eq. (3.26)<sub>3</sub> and Eq. (3.27), gives

$$\rho \vartheta \dot{\eta} = - \text{div } \mathbf{q} + \rho \vartheta \dot{i} \tag{3.30}$$

Operating on the entropy relation, Eq. (3.26)<sub>2</sub>, with the Lie derivative and substituting the result into Eq. (3.30), we obtain

$$\rho c_p \dot{\vartheta} = -\operatorname{div} \mathbf{q} + \vartheta \frac{\rho}{\rho_{Ref}} \frac{\partial \boldsymbol{\tau}}{\partial \vartheta} : \mathbf{d} + \rho \chi^* \boldsymbol{\tau} : \mathbf{d}^p + \rho \chi^{**} \dot{\xi} \quad (3.31)$$

where the specific heat

$$c_p = -\vartheta \frac{\partial^2 \widehat{\psi}}{\partial \vartheta^2} \quad (3.32)$$

and the irreversibility coefficients  $\chi^*$  and  $\chi^{**}$  are determined.

So, the set of constitutive equations of the rate type has the form as follows

$$\begin{aligned} L_{\mathbf{v}} \boldsymbol{\tau} &= \mathcal{L}^e : \mathbf{d} - \mathcal{L}^{th} \dot{\vartheta} - [(\mathcal{L}^e + \mathbf{g} \boldsymbol{\tau} + \boldsymbol{\tau} \mathbf{g}) : \mathbf{P}] \frac{1}{T_m} \left\langle \Phi \left( \frac{f}{\kappa} - 1 \right) \right\rangle \\ \rho c_p \dot{\vartheta} &= -\operatorname{div} \mathbf{q} + \vartheta \frac{\rho}{\rho_{Ref}} \frac{\partial \boldsymbol{\tau}}{\partial \vartheta} : \mathbf{d} + \rho \chi^* \frac{1}{T_m} \left\langle \Phi \left( \frac{f}{\kappa} - 1 \right) \right\rangle \boldsymbol{\tau} : \mathbf{P} + \rho \chi^{**} \dot{\xi} \quad (3.33) \\ \dot{\xi} &= \frac{1}{T_m} h^*(\xi, \vartheta) \left\langle \Phi \left[ \frac{I_n}{\tau_n(\xi, \vartheta, \epsilon^p)} - 1 \right] \right\rangle + \frac{1}{T_m} g^*(\xi, \vartheta) \left\langle \Phi \left[ \frac{I_g}{\tau_n(\xi, \vartheta, \epsilon^p)} - 1 \right] \right\rangle \end{aligned}$$

All the material functions and material constants should be identified based on available experimental data.

### 3.5. Account for shear banding

#### 3.5.1. Microshear banding effects

The derivation of viscoplasticity model accounting for shear banding effects was presented in (cf. Nowak *et al.*, 2007; Perzyna, 2008). Accordingly, the relaxation time  $T_m$  depends on the active microshear bands contribution in the total rate of viscoplastic deformation  $f_{ms}$  and on the rate of equivalent viscoplastic deformation  $\dot{\epsilon}^P$ , i.e.

$$T_m = T_m(f_{ms}, \dot{\epsilon}^P) \quad (3.34)$$

In particular, the above relation takes form

$$T_m = T_m^0 \phi_1(f_{ms}) \phi_2(\dot{\epsilon}^P) \quad (3.35)$$

For example, for DH-36 steel, we can postulate

$$\phi_1(f_{ms}) = [1 - f_{ms}(\epsilon^P)] = \left[ 1 - f_{ms}^0 \frac{1}{1 + \exp(a - b\zeta)} \right] \quad (3.36)$$

and

$$\phi_2(\dot{\epsilon}^P) = \left(\frac{\dot{\epsilon}^P}{\dot{\epsilon}_s^P} - 1\right)^{\frac{1}{m_2}} \tag{3.37}$$

where  $f_{ms}^0$ ,  $a$ ,  $b$  and  $m_2$  are material parameters.

Finally, we have

$$T_m = T_m^0 \left[1 - f_{ms}^0 \frac{1}{1 + \exp(a - b\zeta)}\right] \left(\frac{\dot{\epsilon}^P}{\dot{\epsilon}_s^P} - 1\right)^{\frac{1}{m_2}} \tag{3.38}$$

According to the derivation of the viscoplasticity model accounting for shear banding effects (cf. Nowak *et al.*, 2007), also the isotropic work-hardening-softening function  $\kappa$  depends on the shear banding contribution function  $f_{ms}$

$$\kappa = (1 - f_{ms})^2 \widehat{\kappa}(\epsilon^P, \vartheta, \xi) \tag{3.39}$$

and

$$\kappa = \left[1 - f_{ms}^0 \frac{1}{1 + \exp(a - b\zeta)}\right]^2 \widehat{\kappa}(\epsilon^P, \vartheta, \xi) \tag{3.40}$$

The variable  $\zeta$  takes into account the effect of the type of strain path and its change on the development of shear banding mechanism and its instantaneous contribution to the rate of plastic deformation. In agreement with the study of this problem by Kowalczyk-Gajewska and Pęcherski (2009), the variable  $\zeta$  is given as follows

$$\zeta = \sqrt{\frac{3}{2}} \epsilon^P (1 - \alpha |\cos 3\theta|) \quad 0 \leq \alpha \leq 1 \tag{3.41}$$

$$|\cos 3\theta| = 3\sqrt{6} \left| \det\left(\frac{\mathbf{d}^P}{\|\mathbf{d}^P\|}\right) \right|$$

where  $\alpha$  is a material parameter that describes to what extend the scheme of strain path affects the contribution of microshear banding into the rate of plastic deformation for the considered material.

### 3.6. Fracture criterion based on the evolution of micro-damage and shear banding

We base the fracture criterion on the evolution of the porosity internal state variable  $\xi$ . The volume fraction porosity  $\xi$  takes into account microdamage effects.

Let us assume that for  $\xi = (\boldsymbol{\xi} : \boldsymbol{\xi})^{\frac{1}{2}} = \xi^F$  catastrophe takes place (cf. Perzyna, 1984), that is

$$\kappa = \widehat{\kappa}(\epsilon^P, \vartheta, \xi) \Big|_{(\boldsymbol{\xi} : \boldsymbol{\xi})^{\frac{1}{2}} = \xi^F} = 0 \tag{3.42}$$

It means that for  $(\xi : \xi)^{\frac{1}{2}} = \xi^F$  the material loses its carrying capacity. The above condition describes the main feature observed experimentally that the load tends to zero at the fracture point.

It is noteworthy that the isotropic hardening-softening material function  $\hat{\kappa}$  proposed in Eq. (3.18) should satisfy the fracture criterion Eq. (3.42).

### 3.7. Length-scale sensitivity of the constitutive model

The constitutive equations for a thermo-elastic-viscoplastic model implicitly introduce a length-scale parameter into the dynamic initial-boundary value problem, i.e.

$$l = \beta c T_m \quad \text{or} \quad l = \beta c T_m^0 \phi_1(f_{ms}) \phi_2(\dot{\epsilon}^P) \quad (3.43)$$

and, as an example, for mild steel we have

$$l = \beta c T_m^0 \left[ 1 - f_{ms}^0 \frac{1}{1 + \exp(a - b\zeta)} \right] \left( \frac{\dot{\epsilon}^P}{\dot{\epsilon}_s^P} - 1 \right)^{\frac{1}{m_2}} \quad (3.44)$$

where  $T_m$  is the relaxation time for mechanical disturbances, and is directly related to the viscosity of the material,  $c$  denotes the velocity of the propagation of the elastic waves in the problem under consideration, and the proportionality factor  $\beta$  depends on the particular initial-boundary value problem and may also be conditioned on the microscopic properties of the material.

The relaxation time  $T_m$  can be viewed either as a microstructural parameter to be determined from experimental observations or as a mathematical regularization parameter.

It is noteworthy to stress that the length-scale sensitivity of the constitutive structure is of great importance for proper description of mesomechanical problems.

## 4. Identification procedure

### 4.1. Assumption of the material functions for adiabatic process

To do the proper identification procedure, we first make an assumption on the material functions. In order to simplify the numerical considerations, in this paper we consider strain driven processes without the evolution equation for the porosity  $\xi$ .

The plastic potential function  $f$  is assumed in the form (cf. Perzyna, 1984; Shima and Oyane, 1976)

$$f = \{J'_2 + [n_1(\vartheta) + n_2(\vartheta)\xi]J_1^2\}^{\frac{1}{2}} \tag{4.1}$$

where for simplicity

$$n_1(\vartheta) = 0 \qquad n_2(\vartheta) = n = \text{const} = 0 \tag{4.2}$$

The isotropic work-hardening-softening function  $\kappa$  for DH-36 steel is postulated as (cf. Klepaczko *et al.*, 2009)

$$\kappa = \widehat{\kappa}(\epsilon^P, \vartheta) = \{A + B(\epsilon^P)^n\}[1 - \overline{\vartheta}^{m_3}] \tag{4.3}$$

where

$$\overline{\vartheta} = \frac{\vartheta - \vartheta_0}{\vartheta_m - \vartheta_0}$$

The overstress function  $\Phi((f/\kappa) - 1)$  is assumed in the form (cf. Perzyna, 1963)

$$\Phi\left(\frac{f}{\kappa} - 1\right) = \left(\frac{f}{\kappa} - 1\right)^{m_1} \tag{4.4}$$

The dynamic yield condition for the overstress function  $\Phi$  Eq. (4.4) takes the form

$$\kappa = \widehat{\kappa}(\epsilon^P, \vartheta) = \{A + B(\epsilon^P)^n\} \left[1 - T_m \left(\frac{\epsilon^P}{\dot{\epsilon}^P}\right)^{\frac{1}{m_1}}\right] [1 - \overline{\vartheta}^{m_3}] \tag{4.5}$$

As in the infinitesimal theory of elasticity, we assume linear properties of the material, i.e.

$$\mathcal{L}^e = 2\mu \mathbf{l} + \lambda(\mathbf{g} \otimes \mathbf{g}) \tag{4.6}$$

where  $\mu$  and  $\lambda$  denote the Lamé constants. The thermal expansion matrix is postulated as

$$\mathcal{L}^{th} = (2\mu + 3\lambda)\theta \mathbf{g} \tag{4.7}$$

where the thermal expansion constant e.g. for steel  $\theta = 48 \text{ W/m}^\circ\text{C}$ .

#### 4.2. Determination of material constants

To determine the material constants assumed, we take advantage of the experimental observations presented by Nemat-Nasser and Guo (2003). They investigated the termomechanical response for steel specimens simulating compression processes. The material used in their study was structural steel DH-36 tested over a wide range of strain rates and temperatures. DH-36 steel is a high

**Table 1.** Chemical composition of DH-36 steel Nemat-Nasser and Guo (2003); components defined in wt%

Name	C	Mn	Cu	Si	Cr	Mo
DH-36	0.14	1.37	0.14	0.22	0.08	0.03
Name	V	Ti	Al	Nb	P	S
DH-36	0.001	0.003	0.017	0.03	0.007	0.001

strength structural steel used in naval constructions. The chemical composition of this material after Nemat-Nasser and Guo (2003) is given in Table 1.

Let us now consider an adiabatic dynamic process for a thin steel plate under condition of plane stress state and assume an elastic-plastic model of a material. Additionally, we assume a material of the specimen DH-36 steel and we simplify the considered adiabatic process by postulating that the evolution equation for temperature Eq. (3.33)<sub>2</sub> has the form

$$\dot{\vartheta} = \frac{\chi}{c_p} \boldsymbol{\tau} : \mathbf{d}^p \quad (4.8)$$

i.e. we postulate  $\chi^{**} = 0$ ,  $\chi^* = \chi$  and we neglect the nondissipative term. In fact, we idealize the initial-boundary value problem investigated by Nemat-Nasser and Guo (2003) and by Nowacki *et al.* (2006) by assuming the velocity driven adiabatic process for a thin steel plate. The problem has been solved by using the finite element method.

Based on these assumptions we proceed calculations similarly as in previous paper of Klepaczko *et al.* (1999). For the experimental results of Nowacki *et al.* (2007) and Nemat-Nasser and Guo (2003), we assume that the response is described by Eq. (4.4) and determine the parameters by the method of least squares. The method of least squares requires the residual sum in stress between the experimental observations and model prediction to be minimized. For DH-36 steel, the quasistatic stress-strain curve looks like that in Fig. 8, and the determined constants are presented in Table 2.

**Table 2.** Constants determined for DH-36 steel for Perzyna's model

A	B	n (-)	$T_m^0$	$\dot{\epsilon}_s^P$	$m_1$	$m_2$	$m_3$	$\vartheta_0$	$\vartheta_m$
[MPa]	[MPa]	[-]	[s]	[s <sup>-1</sup> ]	[-]	[-]	[-]	[K]	[K]
810	1130	0.4	$5 \cdot 10^{-6}$	0.001	3.45	12.5	0.32	50	1773

All the material constants has been determined for an adiabatic process and are presented in Table 3.

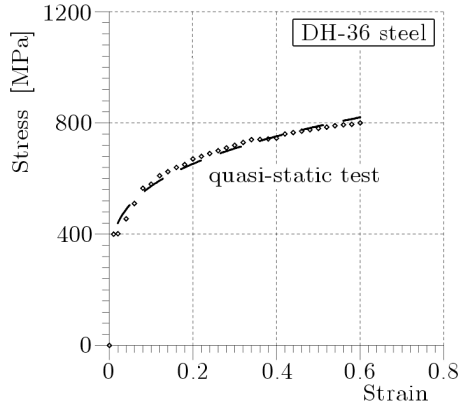


Fig. 8. Quasi-static compression stress-strain relation for DH-36 steel; the dashed line Eq (4.5),  $\diamond$  marks the experimental results by Nemat-Nasser and Guo (2003)

**Table 3.** An DH-36 steel material constants for an adiabatic process

$m_1 = 3.45$	$\vartheta = 293 \text{ K}$	$v = 0.3$
$m_2 = 12.5$	$n=0.4$	$E = 208 \text{ GPa}$
$m_3 = 0.32$	$T_m^0 = 5 \mu\text{s}$	$\rho_{Ref} = 7850 \text{ kg/m}^3$
$\theta = 48 \text{ W/m}^\circ\text{C}$	$\chi = 0.9$	$c_p = 455 \text{ J/kg K}$

### 5. Numerical example

We analyse the impact loaded plate (Fig. 3a). The material of the plate is DH-36 steel modelled as a elasto-viscoplastic material with isotropic hardening effects. We assume that the material softening is caused by the adiabatic mechanism. The height of one shear zone in our sample is equal to 3 mm, width is 20 mm and thickness is 0.64 mm. The plane stress state is considered. As it is shown in Fig. 9, this specimen is loaded symmetrically to the sample axis. Similar boundary value problems for plates were analysed numerically by Klepaczko *et al.* (1999).

To obtain the solution to the initial-boundary value problem formulated, the finite element method for regularized elasto-viscoplastic model has been used<sup>2</sup>. The loading condition is modelled by the velocity of nodes lying on the edge section in center with length of 20 mm, according to the relation

---

<sup>2</sup>Numerical modelling of localized fracture phenomena in inelastic solids in dynamic loading processes by means of the finite element method was presented by Łodygowski and Perzyna (1997).

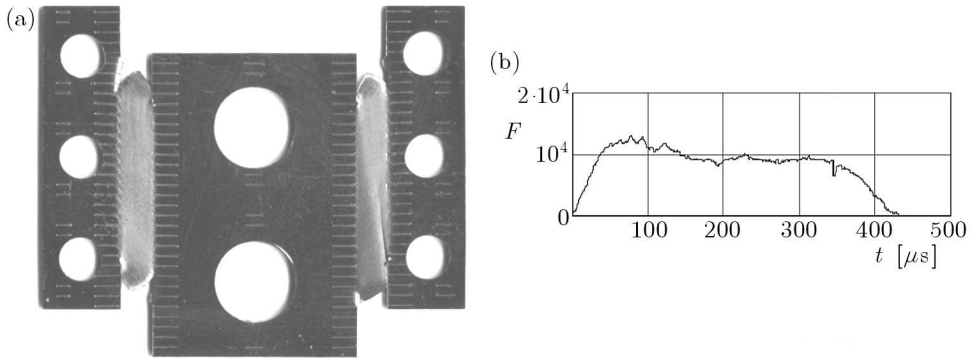


Fig. 9. Experimental dynamic test of DH-36 steel; (a) deformed sample, (b) axial force versus time

$$V(t) = \begin{cases} V_0 \frac{t}{t_r} & \text{for } t \leq t_r \\ V_0 & \text{for } t_r \leq t \leq t_c \\ V_0 - V_0 \frac{t - t_c}{t_e - t_c} & \text{for } t > t_c \end{cases} \quad (5.1)$$

The rise time  $t_r$  is fixed at  $50.0 \mu\text{s}$ ,  $t_c = 340 \mu\text{s}$ ,  $t_e = 440 \mu\text{s}$  and the speed impact  $V_0 = 19.7 \text{ m/s}$ . The initial conditions of the problem are homogeneous. In the discussion of the numerical results, the attention is mostly focused on the phenomenon of localized shear bands.

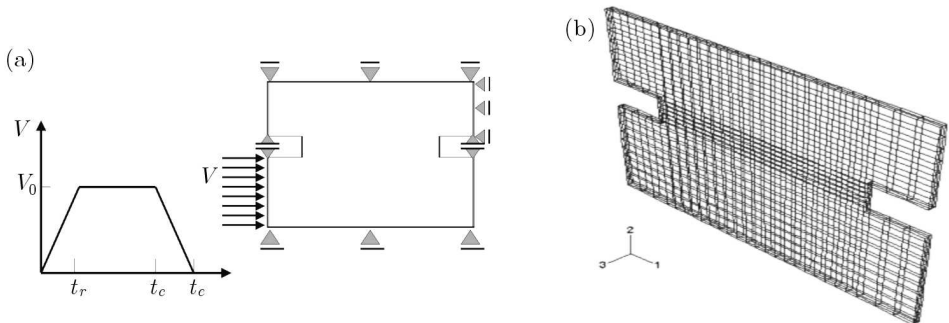


Fig. 10. (a) The impact velocity diagram and the loading condition, (b) the shape of half of the specimen and initial mesh (5226 C3D8R elements)

The finite element ABAQUS program with the explicit time integration scheme (conditionally stable) is used. The stress state in a nodal environment is determined by the iterative procedure of solving the dynamical yield condition

with respect to the norm of the plastic deformation rate tensor. We assume a nonuniform mesh of nodes which contain 7 488 nodes. The smallest size of mesh has the dimensions  $\Delta\Upsilon^1 = 200 \mu\text{m}$  and  $\Delta\Upsilon^3 = 213 \mu\text{m}$ , the time increment  $\Delta t = 0.0356 \mu\text{s}$ . The mesh is shown in Fig. 10b.

### 5.1. Numerical results for simple shearing

The shear band region which undergoes significant deformation has been analysed numerically. Its evolution until the occurrence of final fracture has been simulated. The shear band advance as a function of time has been determined. Our numerical simulation of the dynamic initial boundary value problem enables qualification of the local strain as a local fracture strain.

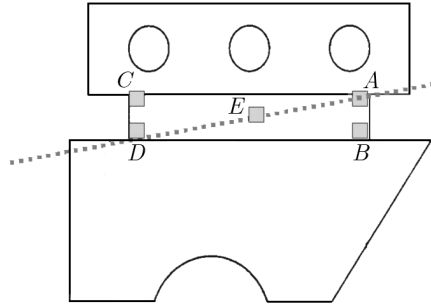


Fig. 11. A pattern of points for presentation of the results

A qualitative comparison of the numerical results with experimental observation data prove the usefulness of the elasto-plastic and elasto-viscoplastic theories in the numerical investigation of rate dependent dynamic fracture. The numerical solution results for the initial velocity  $V = 19.7 \text{ m/s}$  is shown in Fig. 12. In Fig. 12, the distribution of temperature in the shear band region for  $t = 340 \mu\text{s}$  and the evolution of temperature in selected points indicated in Fig. 11 are presented.

From Fig. 12 we can observe a very exact shear band and the initiation of fracture region in the finally deformed specimen.

The modelling of the localized fracture in high strength steels can be examined, and the influence of impact velocity on local failure can be determined. Repeating the tests for different impact velocities, we can find the dependence of local fracture strain on the rate of deformation.

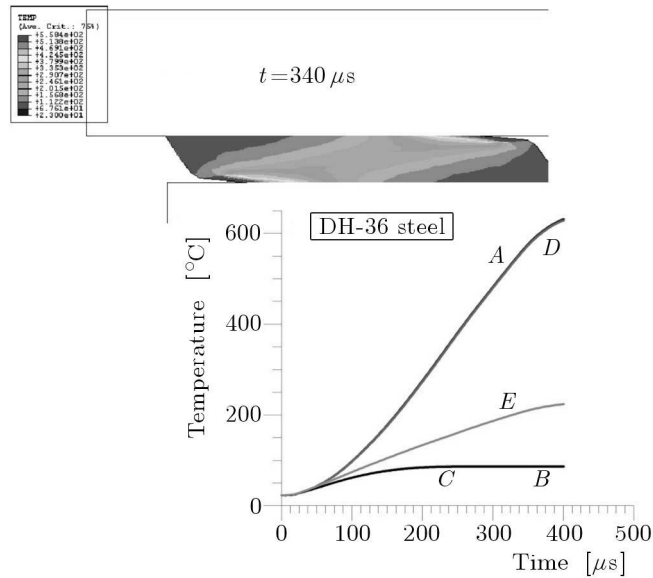


Fig. 12. A contour plot of temperature distribution for  $t = 340 \mu s$  in the shear region and the temperature evolution in the pattern of points versus time of the shear process

## 6. Conclusions

Concluding the presented discussion and analysis, the following outline of a new methodology of analysing the effect of strain rate on ductile fracture can be proposed. It consists of the steps as follows:

- (i) experimental determination of stress-strain characteristics of a material (e.g. DH3-steel) under quasi-static and dynamic loading conditions, in tension, compression or simple shear tests associated with registration *in situ* of temperature evolution and microstructural observations of deformed and damaged specimens,
- (ii) numerical simulation of the investigated processes to identify the viscoplasticity model accounting for shear banding with use of additional data obtained from a thermovision camera and to simulate the tests until fracture initiation,
- (iii) calculation of the evolution of equivalent strain and local strain rate at the critical site of the specimen (detected during the test with use of the thermovision camera),

- (iv) determination of the fracture strain from the comparison between the experimentally registered force-displacement curve and numerical simulations,
- (v) analysis of the effects of strain rate by means of the sequence of numerical simulations of the dynamic tests performed with variable initial velocity.

The aforementioned outline presents in fact a broad research program which requires long-term investigations and cooperation of several research laboratories devoted to the solution of the discussed question of the strain-rate effect on ductile fracture. Realisation of such a program would be at the same time the fulfilment of the scientific heritage of our late Colleague and Friend Wojciech Krzysztof Nowacki.

#### *Acknowledgement(s)*

The research reported in the paper was obtained in the framework of the research project NN501 036435 of the Ministry of Science and Higher Education of Poland.

### References

1. ARIAS A., RODRÍGUEZ-MARTÍNEZ J.A., RUSINEK A., 2008, Numerical simulations of impact behaviour of thin steel plates subjected to cylindrical, conical and hemispherical non-deformable projectiles, *Engineering Fracture Mechanics*, **75**, 1635-1656
2. CURRAN D.R., SEAMAN L., SHOCKEY D.A., 1987, Dynamic failure of solids, *Physics Reports*, **147**, 253-388
3. DORNOWSKI W., PERZYNA P., 2000, Localization phenomena in thermoviscoplastic flow processes under cyclic dynamic loadings, *Computer Assisted Mechanics and Engineering Sciences*, **7**, 117-160
4. DUSZEK-PERZYNA M.K., PERZYNA P., 1994, Analysis of the influence of different effects on criteria for adiabatic shear band localization in inelastic solids, In: *Material Instabilities: Theory and Applications*, R.C. Batra and H.M. Zbib (Eds.), ASME Congress, Chicago, AMDVol.183/MDVol.50, ASME, New York, 59-85
5. FRAŚ T., NOWAK Z., PERZYNA P., PEŁCHERSKI R.B., 2010, Identification of the model describing viscoplastic behaviour of high strength metals, *Inverse Problems in Science and Engineering*
6. GARY G., NOWACKI W.K., 1994, Essai de Cisaillement Plan Dynamique Appliquée a des Tôles Mincees, *Journal de Physique IV*, **C8**, 65-70

7. JOHNSON J.N., 1981, Dynamic fracture and spallation in ductile solids, *J. Appl. Phys.*, **52**, 2812-2825
8. KELVIN L., 1853, On the thermoelastic and thermo-magnetic properties of matter, *Trans. Roy. Soc. Edinb.*, **20**, 161, 57-77
9. KLEPACZKO J.R., NGUYEN H.V., NOWACKI W.K., 1999, Quasi-static and dynamic shearing of sheet metals, *Eur. J. Mech. A/Solids*, **18**, 271-289
10. KLEPACZKO J.R., RUSINEK A., RODRÍGUEZ-MARTÍNEZ J.A., PEŁCHERSKI R.B., ARIAS A., 2009, Modelling of thermo-viscoplastic behaviour of DH-36 and Weldox 460-E structural steels at wide ranges of strain rates and temperatures, comparison of constitutive relations for impact problems, *Mech. Mater.*, **41**, 599-621
11. KOWALCZYK-GAJEWSKA K., PEŁCHERSKI R.B., 2009, Phenomenological description of the effect of microshear banding in micromechanical modelling of polycrystalline plasticity, *Archives of Metallurgy and Materials*, **54**, 1145-1156
12. ŁODYGOWSKI T., PERZYNA P., 1997, Numerical modelling of localized fracture of inelastic solids in dynamic loading processes, *Int. J. Num. Meth. Engng.*, **40**, 4137-4158
13. MARSDEN J.E., HUGHES T.J.R., 1983, *Mathematical Foundations of Elasticity*, PrenticeHall, Englewood Cliffs, New York
14. NEMAT-NASSER S., GUO W.G., 2003, Thermomechanical response of DH-36 structural steel over a wide range of strain rates and temperatures, *Mech. Mat.*, **35**, 1023-1047
15. NOWACKI W.K., GADAJ S.P., LUCKNER J., NOWAK Z., PERZYNA P., PEŁCHERSKI R.B., 2007, Effect of strain rate on ductile fracture, *Report of the Award No FA 8655-05-1-3049 from the European Office of Aerospace Research and Development*
16. NOWACKI W.K., 2001, Dynamic simple shear of sheets at high strain rates, In: *Impact Engineering and Application, Proc. of 4<sup>th</sup> International Symposium on Impact Engineering*, Elsevier, 83-90
17. NOWAK Z., PERZYNA P., PEŁCHERSKI R.B., 2007, Description of viscoplastic flow accounting for shear banding, *Archives of Metallurgy and Materials*, **52**, 217-222
18. PERZYNA P., 1963, The constitutive equations for rate sensitive plastic materials, *Quart. Appl. Math.*, **20**, 321-332
19. PERZYNA P., 1966, Fundamental problems in viscoplasticity, *Advances in Applied Mechanics*, **9**, 343-377
20. PERZYNA P., 1984, Constitutive modelling of dissipative solids for postcritical behaviour and fracture, *ASME J. Eng. Materials and Technology*, **106**, 410-419

21. PERZYNA P., 1986, Internal state variable description of dynamic fracture of ductile solids, *Int. J. Solids Structures*, **22**, 797-818
22. PERZYNA P., 1995, Interactions of elasticviscoplastic waves and localization phenomena in solids, *Proc. of IUTAM Symposium on Nonlinear Waves in Solids*, August 15-20, 1993, Victoria, Canada; J.L. Wegner and F.R. Norwood (Eds.), ASME, 114-121
23. PERZYNA P., 2005, The thermodynamical theory of elasto-viscoplasticity. Review paper, *Engineering Transactions*, **53**, 235-316
24. PERZYNA P., 2008, The thermodynamical theory of elastoviscoplasticity accounting for microshear banding and induce anisotropy effects, *Mechanics*, **27**, 25-42
25. PĘCZERSKI R.B., 1998, Macroscopic effect of microshear banding in plasticity of metals, *Acta Mechanica*, **131**, 203-224
26. RUSINEK A., GADAJ S.P., NOWACKI W.K., KLEPACZKO J.R., 2002, Simulation of heat exchange during simple shear of sheet steel, *Journal of Theoretical and Applied Mechanics*, **40**, 2, 317-337
27. SHIMA S., OYANE M., 1976, Plasticity for porous solids, *Int. J. Mech. Sci.*, **18**, 285-291
28. YOSHIDA K., MYAUCHI K., 1978, Experimental studies of mechanical behaviour as related to sheet metal forming, In: *Mechanics Sheet Metal Forming*, Plenum Press, New York, 19-49

## **Nowa metoda analizy wpływu prędkości odkształcenia na zniszczenie plastyczne metali**

### Streszczenie

W pracy przedstawiono nowy sposób analizy zjawiska zniszczenia ciągliwego metali z uwzględnieniem wpływu prędkości odkształcenia. Przedstawiono teorię materiałów niesprężystych z uwzględnieniem efektu pasm ścinania i mikrouszkodzeń. W opisie zjawiska płynięcia plastycznego uwzględniono wpływ mikropasm ścinania przez wprowadzenie funkcji opisującej chwilowy udział mikropasm ścinania w całkowitej prędkości deformacji plastycznej. Przedstawiono wyniki badań doświadczalnych określających wpływ prędkości odkształcenia na zniszczenie i sposób wykorzystania obserwacji termograficznych w dynamicznej próbie podwójnego ścinania dla stali DH-36. Pomiarzy zmian temperatury podczas procesu deformacji dostarczają dodatkowych danych ułatwiających zidentyfikowanie funkcji udziału mikropasm ścinania dla danego materiału.